Quantitative Determination of Contributions to the Thermoelectric Power Factor in Si Nanostructures

Hyuk Ju Ryu, Z. Aksamija, D. M. Paskiewicz, S. A. Scott, M. G. Lagally, I. Knezevic, and M. A. Eriksson
University of Wisconsin-Madison, Madison, Wisconsin 53706, USA
(Received 16 March 2010; published 13 December 2010)

We report thermoelectric measurements on a silicon nanoribbon in which an integrated gate provides strong carrier confinement and enables tunability of the carrier density over a wide range. We find a significantly enhanced thermoelectric power factor that can be understood by considering its behavior as a function of carrier density. We identify the underlying mechanisms for the power factor in the nanoribbon, which include quantum confinement, low scattering due to the absence of dopants, and, at low temperatures, a significant phonon-drag contribution. The measurements set a target for what may be achievable in ultrathin nanowires.

DOI: 10.1103/PhysRevLett.105.256601 PACS numbers: 72.20.Pa, 73.50.Lw, 73.63.−b, 85.35.−p

Highly doped semiconductors are the class of thermoelectric materials with the highest figure of merit [1,2]. The figure of merit ZT is a composite equal to $S^2T/\rho\kappa$, where S is the thermopower, ρ is the electrical resistivity, κ is the thermal conductivity, and T is the operating temperature. In semiconductors, the power factor S^2/ρ and the thermal conductivity κ are largely decoupled [3]. The power factor is governed by charge carrier transport, and it is well known that it can be increased with doping, until high doping levels are reached [4,5]. In contrast, thermal transport is governed largely by phonon scattering. Good thermoelectric materials have small κ, which in principle can be accomplished without a significant degradation of electronic properties, such as the power factor. (This approach is often referred to as the "electron-crystal, phonon-glass" approach [3]). Reduced κ is achievable through alloying, surface roughening [6,7], or incorporating structural heterogeneities [8,9]. Recently, silicon nanowires and nanoribbons have emerged as promising thermoelectric materials [10,11], because of reduced thermal conductivity caused by phonon scattering at rough boundaries. In this context, it is important to understand how the power factor in silicon nanostructures can be maximized, a process that should ideally make use of high carrier densities and quantum confinement [12].

In this Letter, we report thermoelectric measurements on a silicon nanoribbon with an integrated back gate. Such a gate, while precluding the measurement of thermal conductivity, enables tuning the carrier density in a single device and simultaneously provides strong carrier confinement. Using this approach, we find a significantly enhanced thermoelectric power factor, relative to what has been earlier achieved. We can understand the enhancement by considering the behavior of the power factor as a function of carrier density and temperature. We identify the underlying mechanisms for the large power factor, which include enhancements due to quantum confinement, low carrier scattering due to the absence of dopants, and, at low temperatures, significant phonon drag of up to 46% of the total thermopower. The measurements and modeling demonstrate that strong quantum confinement and high carrier density can indeed enhance the power factor in confined Si structures, consistent with long-standing theoretical predictions [12]. Thus, our measurements set a target for what may be achievable in ultrathin nanowires.

Figure 1 shows a scanning electron micrograph of a thermoelectric device formed from an individual gated nanoribbon of thickness 20 nm. The device is fabricated from (110) silicon-on-insulator (SOI) using electron beam lithography and reactive ion etching with SF_6 and O_2 gases. The nanoribbon is oriented along the high-hole-mobility $[\bar{1}10]$ direction. The green-shaded Ni wires act as thermometers and electrical contacts to the nanoribbon,

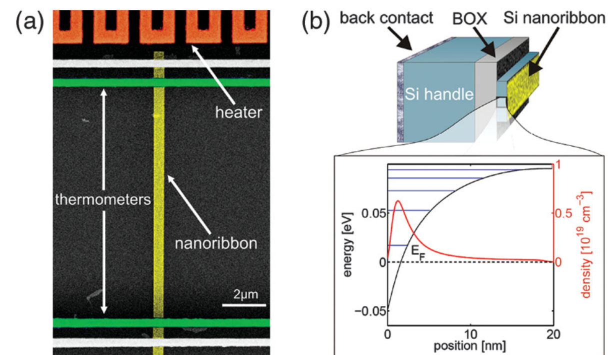

FIG. 1 (color). Gated Si nanoribbon thermoelectric device. (a) Colorized scanning electron micrograph of a device with the same structure as the one measured here. The surface is (110), and the nanowire is oriented along the $[\bar{1}10]$ direction. (b) Perspective schematic diagram of the sample. Inset: The red curve shows the charge distribution in the nanoribbon when the sheet density $n_s = 2.15 \times 10^{12}$ cm^{-2}. The horizontal lines are the subbands derived from the heavy-hole band; the subbands derived from the light-hole and split-off bands are omitted from the plot, for clarity. The Fermi level is at zero energy.

 © 2010 The American Physical Society

and are patterned with electron beam lithography, followed by O_2 plasma cleaning, an HF dip, 110-nm-thick nickel deposition by electron beam evaporation, and annealing at 220 °C for 5 min in forming gas. In the measurements discussed below, there will be some temperature drop at the metal-semiconductor contacts. This effect is minimized by the geometry of the contacts, which are in parallel with the heat flow rather than in series with it [13]. We also use contacts that are the same on both ends of the ribbon, to maximize symmetry, because any temperature offset that is the same on both sides will cancel out in the analysis. The orange-shaded integrated heater is visible at the top of the image. The width and length of the nanoribbon are $W = 420$ nm and $L = 10$ μm, respectively. A back gate enables *in situ* tuning of the carrier density [Fig. 1(b)].

Figure 2 shows the experimentally obtained hole thermopower S as a function of the back-gate bias V_g (the top axis). As the back-gate voltage decreases, the measured thermopower increases dramatically. Further, the mobility remains high over this gate voltage range, as shown by the blue curve in Fig. 3(a). The combination of this strong thermopower and high mobility is a very large power factor, as shown in Fig. 4(a).

To understand these results, it is very useful to compare to theory, and such a comparison is best made by looking at the dependence of the thermopower and power factor on carrier density and temperature. Such a task has been very challenging in doped nanostructures, because their large surface-to-volume ratios mean that interface traps significantly reduce the effective carrier density [14], while simultaneously making that carrier density difficult to measure.

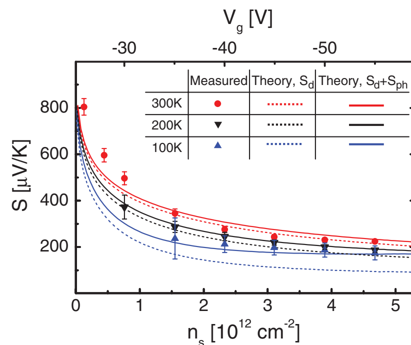

FIG. 2 (color). Thermopower of holes in a gated silicon nanoribbon as a function of n_s and V_g at $T = 300$ K (red), 200 K (black), and $T = 100$ K (blue). Symbols are the measurement; the curves are calculated values (dashed line: diffusion thermopower only, solid line: diffusion and phonon-drag thermopowers combined). During the measurement, the temperature difference $\triangle T$ induced across the nanoribbon is typically below 2 K, and the thermoelectric voltage is measured using a nanovoltmeter with input impedance exceeding 10 GΩ. The contribution from the nickel electrodes [30] is subtracted from the results, and it is less than 5% of the total thermopower in all cases.

For the gated nanoribbon we consider here, the carrier density of interest is the two-dimensional sheet density n_s. To determine n_s, we first perform Hall measurements as a function of V_g on a very wide ribbon ($W \times L = 50$ μm $\times$ 500 μm), patterned on SOI with a thickness the same as the nanoribbon to within ± 1 nm [Fig. 3(a)]. The measured hole mobility is close to that of bulk MOSFETs [15,16], and it is nearly constant as a function of gate voltage, which is indicative of the relatively low importance of surface-roughness scattering for hole transport in this density range [17]. The temperature dependence of the hole mobility, shown in the inset to Fig. 3(a), implies that phonon scattering dominates transport in this regime [18].

Because the threshold voltage V_{th} will differ for the wide ribbon and the nanoribbon, due to traps and fixed charge in the ribbon faces [19,20], we determine the threshold difference $\delta V_{th} = -14$ V between the nanoribbon and the wide ribbon from the shift in the transconductance, as shown in Fig. 3(b). In the above-threshold linear regime, the sheet density n_s is linearly proportional to the gate voltage: $n_s = C_{ox}(V_g - V_{th})/q$, and the results of this mapping are shown on the bottom axis in Fig. 2. This method is most accurate in the linear regime above threshold, which includes the majority of the gate voltage range presented here.

In order to understand the large thermopower and power factor measured here, we perform calculations of the total thermopower, including both charge diffusion and phonon drag. The expression for the diffusion thermopower S_d is derived from the 2D Boltzmann transport equation (BTE) under the effective-mass and relaxation time approximations (RTA). At a temperature T, the conductivity σ and the diffusion thermopower S_d are given by [21]

$$\sigma = L^{(0)}, \qquad S_d = \frac{1}{qT}\frac{L^{(1)}}{L^{(0)}}, \tag{1}$$

where the generalized transport matrix element $L^{(j)}$ is given by

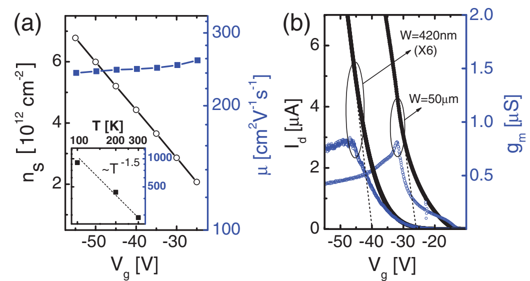

FIG. 3 (color). Characterization of hole sheet density n_s and mobility μ. (a) n_s and μ as a function of the gate voltage, obtained from Hall measurements on a wide ribbon ($W \times L = 50$ μm $\times$ 500 μm). Inset: Hole mobility as a function of temperature at $V_g = -55$ V. (b) Black curves: $I_d - V_g$ characteristics of the nanoribbon and the 50 μm-wide ribbon, both at a source-drain voltage of 1 V. Blue curves: transconductance g_m.

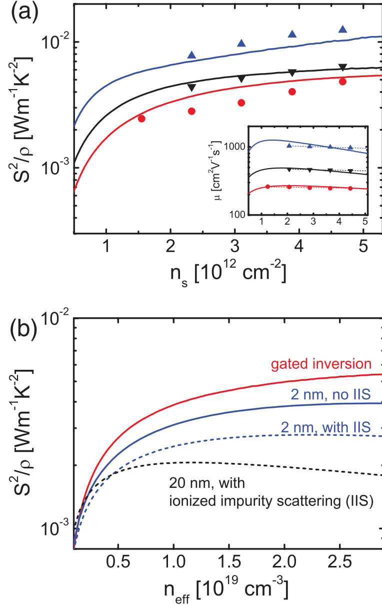

FIG. 4 (color). Power factor S^2/ρ. (a) Solid symbols show the power factor at $T = 300$ (red), 200 (black), and 100 K (blue). Solid curves show the total calculated power factor, including both diffusion and phonon-drag components. Inset: mobility μ as a function of n_s; solid lines: calculation; dashed lines: linear fit. (b) S^2/ρ as a function of the effective three-dimensional hole density n_{eff} at $T = 300$ K for four cases. Dashed black: doped nanoribbon of thickness 20 nm. Dashed blue: doped nanoribbon of thickness 2 nm. Solid blue: doped nanoribbon of thickness 2 nm with ionized impurity scattering (IIS) removed from the calculation. Solid red: gated nanoribbon corresponding to the experiment. For the cases with doping, $n_{\text{eff}} = N_A$; for the gated nanoribbon, $n_{\text{eff}} = n_s/w$, where w is the effective thickness of the inversion layers, as described in the text.

$$L^{(j)} = \sum_{\nu,i} \frac{2q^2}{m_i^\nu} \int E \frac{\partial f_0(E)}{\partial E}(E - E_F + E_i^\nu)^j \tau_i^\nu(E) g_i^\nu(E) dE. \quad (2)$$

Here, $f_0(E)$ is the Fermi-Dirac distribution function, and E_F is the Fermi level. E_i^ν is the energy of the bottom of subband i in valley ν, $g_i^\nu(E)$ is the density of states, and $\tau_i^\nu(E)$ is the relaxation time of a hole with effective mass m_i^ν and kinetic energy E in that subband. The subband energies and wave functions were calculated by solving the Schrödinger and Poisson equations self-consistently [22]. $1/\tau_i^\nu(E)$, the scattering rate, is a sum of the rates due to all the important scattering mechanisms: acoustic phonons, optical phonons, surface roughness, and charged interface traps [23–25]. A root-mean-square surface roughness of 0.15 nm is used in the calculations. An acoustic-phonon deformation potential of 14 eV gives the best agreement with measured mobility.

The phonon-drag contribution to the thermopower, S_{ph}, arises from hole-phonon scattering in the presence of net flux of phonons from hot to cold. It is calculated from the fraction γ of the total hole scattering rate that corresponds to hole-acoustic-phonon scattering, the average velocity and mean free path of acoustic phonons (v_{ph} and Λ_{ph}, respectively), and the mobility of holes μ [26]:

$$S_{\text{ph}} = \frac{\gamma v_{\text{ph}} \Lambda_{\text{ph}}}{\mu T}. \quad (3)$$

Because the hole mobility in inversion layers is largely phonon limited up to very high densities [17] [see Fig. 3(a)], we assume $\gamma = 1$.

Figure 2 shows the calculations of the thermopower at the same three temperatures for which data are presented. The dashed curves are the diffusion thermopower alone, whereas the solid curves are the sum of the diffusion and phonon-drag thermopowers. The agreement between experiment and theory is very good, especially at higher carrier densities where the calibration between V_g and n_s is most accurate. The diffusion thermopower decreases as n_s increases, following an approximate $\sim 1/n_s$ trend. The phonon-drag contribution, the difference between the solid and dashed curves, is roughly 8.3% of total at 300 K, and it is up to 46% of total at 100 K. This increase in importance of phonon drag at lower temperature is caused by the increase in the phonon mean free path with decreasing temperature.

Figure 4(a) shows the power factor S^2/ρ of the nanoribbon as a function of sheet density and gate voltage. We use the calculated thickness of the hole inversion layer, which we obtain from the full-width at half-maximum of the charge density profile, to convert the 2D sheet resistance into a resistivity ρ. The power factor increases significantly with increasing carrier concentration. At $T = 100$ K, phonon drag makes a significant contribution to the power factor. This contribution is most significant at high density, because S_{ph} does not decrease with increasing n_s. Thus, thanks to the near independence of S_{ph} on n_s, by increasing n_s one can decrease ρ while still maintaining a sizable $S = S_d + S_{\text{ph}}$, resulting in a large power factor S^2/ρ.

To understand the increase in power factor at higher temperatures, we perform calculations of the power factor in a series of ribbons, varying several essential parameters one at a time. In Fig. 4(b), the dashed black line shows S^2/ρ for an ungated 20 nm-thick nanoribbon. The charge density is assumed to arise from doping, and we include scattering with the ionized dopant atoms when calculating the mobility μ. The power factor peaks around $n_{\text{eff}} \sim 1 \times 10^{19}$ cm^{-3}, and it falls off at higher densities as dopant scattering reduces the mobility. The dashed black curve is similar to that expected for bulk and provides a baseline for comparison.

The dashed blue curve in Fig. 4(b) shows an identical calculation, but with the ribbon thickness reduced to 2 nm, approximately equal to the thickness of the inversion layer for the data presented here. The power factor is significantly larger, because of the beneficial effects of quantum confinement [12,27]. However, dopant scattering still

causes a reduction in mobility at higher doping densities. The solid blue curve shows the result of removing dopant scattering "by hand," something that can only be done using theory; the result is another significant step up in the power factor. In a real physical system, providing a carrier density without dopants requires a gate, and the calculation corresponding to such a situation is shown as the red line, which is a good match with the points for the gated nanoribbon.

The power factor of the gated nanoribbon is higher than that reported for heavily doped silicon nanowires [11], which do not achieve values as high as those in Fig. 4(a), even at nominal dopant densities that far exceed the nanoribbon effective carrier density range studied here. We believe that interface traps make the actual charge density in such wires far lower than expected from the nominal dopant density. Further, the mobility is suppressed because the density of scattering centers far exceeds the density of free carriers, suppressing the power factor even more. In contrast, gate tuning offers control of the carrier density in nanostructures in a way that does not significantly affect scattering rates.

To summarize, we have presented measurements and calculations of the hole thermopower and power factor in gated silicon $[\bar{1}10]/(110)$ nanoribbons. With increasing sheet density, tuned by a back gate, the power factor of the nanoribbons is significantly enhanced, because of the combined effects of quantum confinement, a hole mobility that does not decrease with increasing carrier density, and (especially at low T) phonon drag. We have used an essentially metallic gate to demonstrate such enhancements and to facilitate understanding and comparison to theory. In a practical system, recent advances such as surface transfer doping [14,28,29] could be used to provide carriers, in place of either bulk doping or a metallic gate, and in analogy with the field effect of a gate. Critically, such surface transfer doping will also produce a large electric field between the surface and the carriers in the interior of a nanowire, and thus the benefits of quantum confinement are expected to remain in such an approach.

This work was supported by DOE (No. DE-FG02-03ER46028), AFOSR [MURI (No. FA9550-08-1-0337) and YIP programs (No. FA9550-09-1-0230)], and NSF (No. 0937060 subgrant No. CIF-146); D. M. P. acknowledges support from the NSF. The authors thank G. K. Celler, Soitec, Inc. for providing some of the materials used in this study and E. B. Ramayya for many helpful discussions. We acknowledge facilities support from the University of Wisconsin NSF–supported MRSEC.

[1] F. J. DiSalvo, Science **285**, 703 (1999).
[2] A. Majumdar, Nature Nanotech. **4**, 214 (2009).
[3] G. A. Slack, *CRC Handbook of Thermoelectrics* (CRC Press, Boca Raton, FL, 1995), pp. 407–440.
[4] T. Geballe and G. Hull, Phys. Rev. **98**, 940 (1955).
[5] L. Weber and E. Gmelin, Appl. Phys. A **53**, 136 (1991).
[6] R. Chen, A. I. Hochbaum, P. Murphy, J. Moore, P. Yang, and A. Majumdar, Phys. Rev. Lett. **101**, 105501 (2008).
[7] T. Markussen, A.-P. Jauho, and M. Brandbyge, Phys. Rev. Lett. **103**, 055502 (2009).
[8] G. J. Snyder and E. S. Toberer, Nature Mater. **7**, 105 (2008).
[9] R. Venkatasubramanian, E. Siivola, T. Colpitts, and B. O'Quinn, Nature (London) **413**, 597 (2001).
[10] A. I. Hochbaum, R. Chen, R. D. Delgado, W. Liang, E. C. Garnett, M. Najarian, A. Majumdar, and P. Yang, Nature (London) **451**, 163 (2008).
[11] A. I. Boukai, Y. Bunimovich, J. Tahir-Kheli, J. Yu, W. A. Goddard, III, and J. R. Heath, Nature (London) **451**, 168 (2008).
[12] L. D. Hicks and M. S. Dresselhaus, Phys. Rev. B **47**, 12 727 (1993).
[13] C.-H. Lee, G.-C. Yi, Y. M. Zuev, and P. Kim, Appl. Phys. Lett. **94**, 022106 (2009).
[14] P. P. Zhang, E. Tevaarwerk, B. N. Park, D. E. Savage, G. K. Celler, I. Knezevic, P. G. Evans, M. A. Eriksson, and M. G. Lagally, Nature (London) **439**, 703 (2006).
[15] G. Tsutsui and T. Hiramoto, IEEE Trans. Electron Devices **53**, 2582 (2006); http://ieeexplore.ieee.org/xpls/abs_all.jsp?arnumber=1705113&tag=1
[16] H. Irie, K. Kita, K. Kyuno, and A. Toriumi, IEDM Tech. Digest 225 (2004); http://ieeexplore.ieee.org/xpls/abs_all.jsp?arnumber=1419115&tag=1
[17] L. Donetti, F. Gamiz, N. Rodriguez, and A. Godoy, IEEE Electron Device Lett. **30**, 1338 (2009).
[18] A. Teramoto *et al.*, IEEE Trans. Electron Devices **54**, 1438 (2007).
[19] K. Eriguchi and K. Ono, J. Phys. D **41**, 024002 (2008).
[20] J. C. Arnold and H. H. Sawin, J. Appl. Phys. **70**, 5314 (1991).
[21] J. Ziman, *Electrons and Phonons: The Theory of Transport Phenomena in Solids* (Oxford University Press, Inc., New York, 1960).
[22] T. Ando, A. Fowler, and F. Stern, Rev. Mod. Phys. **54**, 437 (1982).
[23] I. Knezevic, E. B. Ramayya, D. Vasileska, and S. M. Goodnick, J. Comput. Theor. Nanosci. **6**, 1725 (2009).
[24] M. V. Fischetti and S. E. Laux, Phys. Rev. B **48**, 2244 (1993).
[25] E. Wang, P. Matagne, L. Shifren, B. Obradovic, R. Kotlyar, S. Cea, M. Stettler, and M. Giles, IEEE Trans. Electron Devices **53**, 1840 (2006).
[26] M. Tsaousidou, P. N. Butcher, and G. P. Triberis, Phys. Rev. B **64**, 165304 (2001).
[27] L. D. Hicks, T. C. Harman, X. Sun, and M. S. Dresselhaus, Phys. Rev. B **53**, R10493 (1996).
[28] T. He, J. He, M. Lu, B. Chen, H. Pang, W. F. Reus, W. M. Nolte, D. P. Nackashi, P. D. Franzon, and J. M. Tour, J. Am. Chem. Soc. **128**, 14 537 (2006).
[29] S. A. Scott, W. Peng, A. M. Kiefer, H. Jiang, I. Knezevic, D. E. Savage, M. A. Eriksson, and M. G. Lagally, ACS Nano **3**, 1683 (2009).
[30] L. Gravier, A. Fabian, A. Rudolf, A. Cachin, K. Hjort, and J. Ansermet, Meas. Sci. Technol. **15**, 420 (2004).